valving was included so that shutoff redundancy is assured to prevent propellant loss in the event of TCA propellant valve malfunction. By using the isolation valve arrangement shown in Fig. 12, a single bipropellant valve could be used on each TCA.

Location of ISPS components on the vehicle aft rack resulted in a seven foot separation of the TCAs and the EMPAs. In addition, the use of the dual EMPA/TCA approach with interconnecting plumbing, created a potential difficulty in propellant bleed in. The resolution to this problem is to keep the system dry on the pad and during ascent by keeping the upstream LSVs closed (system cleanliness is ensured by pressurizing the ISPSs to 20 psia with GN_2 before closing the LSVs). Both systems are bled in on orbit by opening the TCA propellant valves and venting the GN_2. Five minutes is allocated for the systems to be evacuated to space vacuum and then the propellant valves are closed. The upstream LSVs are opened and the propellants flow from the sumps and fill both systems. Six minutes is allocated for filling and is verified by the TCA venturi inlet pressures reading the same values as propellant tank pressures.

System operation is accomplished in the following manner: the pumps are started dead headed and the propellants recirculate through the spill back valves. Four seconds after EMPA start, the TCA propellant valves are commanded open. At the completion of burn, the TCA valves are closed and EMPA motor power interrupted. Pressure rise from thermal expansion of the trapped propellants due to TCA heat soak back is relieved by a relief function in the upstream LSVs which are closed after system operation.

The use of pumps to increase pressures to values compatible with feed pressure requirements of state-of-the-art TCA's required that pump output be approximately 200 psia and that pressure variations be held to plus and minus 5 psi. The selection of a gear pump resulted in 60 psi peak-to-peak variations in pump outlet pressure. Therefore, a pulse attenuator was added to the pump outlet line and reduced pressure amplitudes to acceptable values.

The combination of the EMPA spill back controls and cavitating venturis on the TCAs maintains both mixture ratio and total propellant flowrate within required tolerances. The resulting nominal flowrates of 0.238 lb/sec and 0.089 lb/sec for the HDA oxidizer and USO fuel result in an ISPS mixture ratio of 2.67 which is the same as the Agena main engine. Thus, all available propellant can be used in the ISPS.

While the TCAs have a nominal specific impulse of 273 sec at this mixture ratio the net effective impulse to the vehicle is a nominal 266 sec. This 7 sec reduction is due to axial thrust impingement forces on the main engine nozzle extension and is the minimum value resulting from the ISPS TCA/main engine nozzle extension installation relationships.

NOVEMBER 1974 J. SPACECRAFT VOL. 11, NO. 11

Approximate Impact Dispersion Methods for Symmetric Entry Vehicles

T. D. BURTON*
General Electric Company, Philadelphia, Pa.

Analytical approximations describing symmetric entry vehicle impact dispersions resulting from wind, density, and angle-of-attack statistical effects are derived. Wind and density effects are assessed using a simplified trajectory model and perturbation approach for solution. Simple relations are given for the influence coefficients used in the covariance method calculation of wind and density-induced dispersions. An effective angle of attack induced $1-\sigma$ drag error history is also derived. The results are presented in a form amenable to direct usage in symmetric vehicle impact dispersion assessments. This obviates the need for extensive point mass simulations usually made to obtain the influence coefficient profiles and for Monte Carlo six-degree-of-freedom simulations used to assess the statistical effects of re-entry angle of attack upon dispersion. Approximate and numerically obtained results are compared with good agreement for several values of ballistic coefficient. The results are restricted to the case of ballistic coefficient constant throughout re-entry.

Nomenclature

A = velocity reduction parameter = $g\rho_s/\alpha\beta\sin\gamma$
a_ρ, a_c, a_p = density, crosswind, and parallel-wind influence coefficients, respectively
C_D = drag coefficient
C_{D_1} = incremental drag at angle of attack
$\langle C_{D_1}\rangle$ = mean drag due to angle of attack
σC_{D_1} = $1-\sigma$ drag uncertainty due to angle of attack
$D(h_i, \beta\sin\gamma)$ = density influence coefficient parameter ~ Eq. (26)
g = constant gravitational acceleration
h = altitude
Δh = altitude interval of wind or density perturbation
K = factor in assumed angle of attack drag model, Eq. (37)
q = dynamic pressure, $\frac{1}{2}\rho V^2$
r = distance from spherical earth center to vehicle = R_e+h
r_{ij} = coefficient of correlation between ith and jth levels for winds and density
R_e = Earth radius
R = trajectory range along Earth's surface
S = reference area
V = velocity, Earth relative
$V_{1,e}$ = velocity deviation, initial velocity deviation induced by density error
$V_{x,e}$ = cross range velocity, initial cross range velocity induced by cross wind
V_p = velocity deviation contributing to range dispersion caused by head wind
W = vehicle weight
$w_p, w_\perp$ = parallel and crosswind velocities, respectively
X = cross range
Z = normalized density = ρ/ρ_s

Presented as Paper 74-112 at the AIAA 12th Aerospace Sciences Meeting, Washington, D.C., January 30–February 1, 1974; submitted March 13, 1974; revision received July 11, 1974.

Index categories: Entry Vehicle Dynamics and Control; LV/M Trajectories.

* Supervising Engineer, Flight Dynamics and Simulation Engineering, Re-Entry and Environmental Systems Division.

α = inverse of exponential atmosphere scale height
β = ballistic coefficient = $W/C_D S$
δ = total angle of attack = $(\theta^2+\psi^2)^{1/2}$
δ_m = mean of initial angle of attack Rayleigh distribution
γ = path angle, down from horizontal
λ = total angle of attack attenuation factor
μ, η = drag misalignment due to parallel and cross winds, respectively
ρ, ρ_s = density, reference density for exponential atmosphere
σ = impact range (cross range) error due to density or wind effects, Eq. (1)
σ_i = wind or density statistical error in ith altitude level
θ, ψ = angle of attack components

Subscripts

0 = characteristic of nominal, unperturbed trajectory
1 = represents deviations in trajectory variables due to wind, density, or drag perturbations
e = value at initial re-entry
i = characteristic of altitude h_i or ith altitude interval
L, H = lower and upper altitude bounds of wind perturbation interval

Introduction

THE calculation of impact dispersions is a primary consideration in the design of ballistic re-entry systems. Dispersions occurring during entry through the atmosphere are comprised on the one hand of those deriving for symmetric vehicles, such as wind, density, aerodynamic drag, and initial angle-of-attack statistical effects. Also important is the so called "roll/trim" dispersion resulting for a vehicle possessing mass and configurational asymmetries.[1] In the present investigation only the symmetric vehicle re-entry dispersions are considered.

The effects of wind and density deviations are usually assessed by combining known atmospheric statistical information with sensitivity or "influence" coefficients using the influence coefficient covariance method of Sissenwine,[2] where the $1-\sigma$ impact error is given according to the relation

$$\sigma^2 = \sum_i \sum_i a_i a_j r_{ij} \sigma_i \sigma_j \Delta h_i \Delta h_j \tag{1}$$

The a_i in Eq. (1) are the influence coefficients, defined as the impact error resulting from a unit perturbation applied over a unit altitude interval at h_i. Since drag and density influence coefficients are equal, dispersions resulting from drag uncertainties may also be considered in this way.

The influence coefficient profiles are generally obtained through a large number of point mass trajectory simulations with density or wind perturbations applied over small and successively lower altitude intervals. Similarly, a Monte-Carlo six-degree-of-freedom motion analysis[3] is required in order to assess rigorously the dispersion due to statistical variations in initial re-entry angle of attack.

It would seem desirable for design purposes to eliminate the need for a large number of complex simulations, especially if several entry conditions and vehicle drag characteristics are to be investigated. Through an analytical/empirical analysis Glover[4] has derived simplified expressions for over-all dispersion due to wind and density effects. In the present investigation no attempt is made to provide relations for over-all dispersion. Rather, the influence coefficients are derived in a form which is easily used in the influence coefficient covariance method.

Formulation of Wind and Density Effects

In formulating the trajectory model which is used, several simplifying assumptions have been made in order to realize a tractable system. The altitude h is assumed negligible in comparison to the Earth radius R_e. Winds are assumed present either as horizontal cross or head winds. The vehicle is assumed to rotate instantaneously into the wind with no transient dynamic angle of attack response. Lift forces are considered negligible, so that the only aerodynamic force present is the drag. The assumptions of zero gravity and constant path angle during re-entry

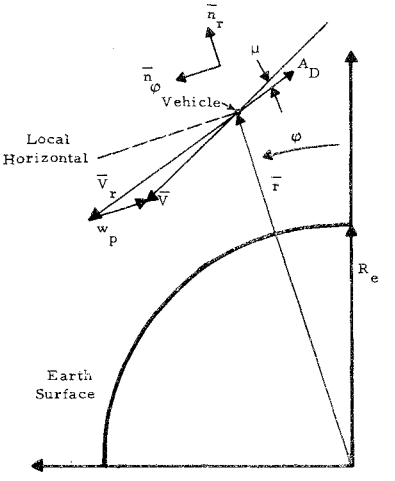

Fig. 1 Definition of trajectory parameters. $\bar{V}_r$ is the wind relative velocity vector.

will be made where necessary to achieve simple results. The final assumption is that the re-entry vehicle ballistic coefficient remains constant throughout entry. This may limit to some extent the applicability of the results but was necessary in order to achieve simple approximations.

The previous assumptions permit the nominal, unperturbed trajectory to be considered two dimensional and independent of location over the Earth. The only out of plane motion that results is that due to a cross wind. In the following, differential equations for velocity, path angle, and range are presented in an altitude dependent form. The density or wind deviation from the nominal is then introduced, and a perturbation analysis about the nominal trajectory is applied in order to establish the resulting range (cross range) impact error and the associated influence coefficients.

The coordinate system used to define the vehicle motion is shown in Fig. 1. A parallel (head) wind will result in a misalignment, defined by the angle μ, of the aerodynamic drag force from the nominal line of flight. A similar misalignment, defined by the angle η, results in the presence of a cross wind. With the coordinates r and ϕ defined as shown, a summation of forces in the radial and tangential directions yields for a point mass re-entry vehicle

$$\ddot{r} - r\dot{\phi}^2 = -g + \frac{qg}{\beta}\sin(\gamma-\mu) \tag{2a}$$

$$r\ddot{\phi} + 2\dot{r}\dot{\phi} = -\frac{qg}{\beta}\cos(\gamma-\mu) \tag{2b}$$

The equation describing out of plane motion due to cross winds is given by

$$\ddot{X} = (qg/\beta)\sin\eta \tag{3}$$

The drag force misalignment angles are determined from the geometry as

$$\eta = \tan^{-1}\left(\frac{w_\perp - \dot{X}}{V}\right); \quad \mu = \sin^{-1}\left(\frac{w_p - V_p}{V}\right)\sin\gamma \tag{4}$$

By noting that $\dot{r} = -V\sin\gamma$ and $r\dot{\phi} = V\cos\gamma$, and using the assumption $r \approx R_e$, Eqs. (2) and (3) are transformed to the altitude domain and rewritten in terms of V, γ, R, X, and V_x as

$$V' = \frac{-g}{V} + \frac{qg\cos\mu}{\beta V\sin\gamma} \tag{5}$$

$$\gamma' = \frac{-g\cos\gamma}{V^2\sin\gamma}\left[1 - \frac{V^2}{gR_e}\right] - \frac{qg\sin\mu}{\beta V^2\sin\gamma} \tag{6}$$

$$R = -\int_{h_0}^{0} (\cos\gamma/\sin\gamma)\,dh \tag{7}$$

$$V_x' = -qg\sin\eta/\beta V\sin\gamma \tag{8}$$

$$X' = -V_x/V\sin\gamma \tag{9}$$

The range R here is understood to be the impact range. These equations form the basis of the trajectory model used herein. If no cross wind is present, Eqs. (5–7) completely specify the

trajectory. Equations such as given above would normally be integrated numerically, trajectory ranges with specified wind and density deviations included being compared to the nominal range in order to establish the influence coefficient magnitudes. In the present investigation, the changes in impact range or cross range resulting from density or wind perturbations will be derived as simple relations which are given in terms of the nominal trajectory variable histories. Thus, the calculation of the influence coefficient profiles could be implemented by the inclusion in standard point mass trajectory simulations of the approximate relations derived subsequently.

Density-Induced Range Errors

The effect of a small deviation in the density over a given altitude interval will be to alter the aerodynamic drag magnitude during that interval. In assessing such an effect only Eqs. (5–7) need be used. It will be assumed that histories of the nominal trajectory variables V_0, γ_0, R_0, and ρ_0 are available. These could be obtained from a point mass trajectory simulation or by utilizing the simplified solutions of Allen and Eggers.[5] Consider, then, a perturbation ρ_1 in the density (applied in some small altitude interval) which results in perturbations, V_1, γ_1, and R_1 in the trajectory variables. The trajectory with perturbation included is defined by a straightforward expansion about the nominal by

$$\begin{aligned} \rho &= \rho_0 + \rho_1 \\ V &= V_0 + V_1 + \cdots \\ \gamma &= \gamma_0 + \gamma_1 + \cdots \\ R &= R_0 + R_1 + \cdots \end{aligned} \tag{10}$$

The assumption that the perturbed trajectory parameters are small relative to the nominal ones is tacit in the above equations, since the influence coefficient approach is a linear analysis. Substitution of Eq. (10) into Eqs. (5–7), application of the small angle assumption for γ_1, neglect of higher-order terms, and use of the small X expansion, $1/(1+X) \approx 1-X$, yields the following system of equations for the perturbed variables, V_1 γ_1, and R_1

$$V_1' = \frac{q_0 g}{\beta V_0 \sin\gamma_0}\left[\frac{\rho_1}{\rho_0} + \frac{V_1}{V_0} - \gamma_1 \cot\gamma_0\right] + \frac{g}{V_0}\left(\frac{V_1}{V_0}\right) \tag{11}$$

$$\gamma_1' = -\frac{g\cot\gamma_0}{V_0^2}\left[-\frac{2V_1}{V_0} - \frac{\gamma_1}{\sin\gamma_0\cos\gamma_0}\left(1 - \frac{V_0^2}{gR_e}\right)\right] \tag{12}$$

$$R_1 = \int_{h_i}^{0} \frac{\gamma_1}{\sin^2\gamma_0}\,dh \tag{13}$$

A solution for the perturbed range R_1 is desired in terms of the perturbing density relative magnitude ρ_1/ρ_0 and the altitude interval Δh_i over which the perturbation appears. The density influence coefficient a_{ρ_i} can then be calculated for the midpoint of the ith altitude interval as

$$a_{\rho_i} = \frac{R_1}{(\rho_1/\rho_0\,\Delta h_i)} \tag{14}$$

Equations (11–13) are coupled and would normally be solved simultaneously. In the present analysis, however, an in-series solution will be attempted by making assumptions regarding the magnitude of various terms in Eqs. (11) and (12). Equation (11) for the perturbed velocity is first solved by assuming that during the interval of the density perturbation, only ρ_1/ρ_0 is significant in that equation. Gravity effects are also neglected, resulting in

$$V_1' \approx \frac{q_0 g}{\beta V_0 \sin\gamma_0}\left(\frac{\rho_1}{\rho_0}\right) \tag{15}$$

which applies during the perturbation interval. The nominal trajectory quantities q_0, V_0, and γ_0 are now assumed constant over the interval, since in the limiting case which defines the influence coefficients, the perturbation interval will be vanishingly small. Equation (15) is then integrated to yield the velocity V_{1_e} at the end of the interval

$$V_{1_e} = \frac{-q_0 g}{\beta V_0 \sin\gamma_0}\left(\frac{\rho_1}{\rho_0}\Delta h\right); \qquad \Delta h > 0 \tag{16}$$

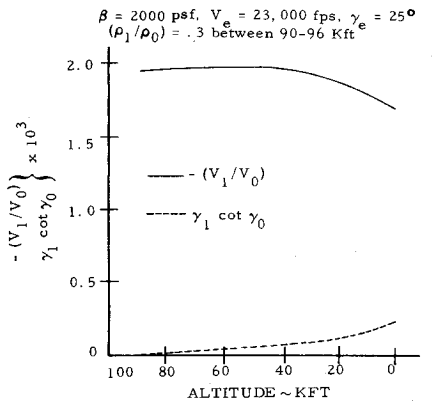

Fig. 2 Comparison of perturbed velocity and path angle terms in Eq. (11).

evaluated at the altitude h_i, where the influence coefficient is to be determined. For altitudes below the perturbation interval, $\rho_1/\rho_0 = 0$, and again neglecting gravity, Eq. (11) becomes

$$V_1' \approx \frac{q_0 g}{\beta V_0 \sin\gamma_0}\left[\frac{V_1}{V_0} - \gamma_1 \cot\gamma_0\right] \tag{17}$$

It will now be assumed that the perturbed velocity ratio (V_1/V_0) is large relative to the term $\gamma_1 \cot\gamma_0$ throughout most of the trajectory. This seems reasonable, since the velocity V_1 is given a more or less impulsive change due to the density perturbation, while the path angle deviation γ_1 builds up very gradually. The assumption has been verified for several cases of interest, and a typical result is shown in Fig. 2. In view of this assumption and Eq. (5) with the gravity term neglected, Eq. (17) can be expressed as

$$V_1'/V_1 \approx V_0'/V_0 \tag{18}$$

which yields the result that the perturbed velocity ratio (V_1/V_0) remains nearly constant during re-entry, as is substantially verified for the specific case shown in Fig. 2. The value of (V_1/V_0) is required in Eq. (12) for the perturbed path angle γ_1 and can be obtained from Eq. (16) as

$$\frac{V_1}{V_0} \approx -\frac{\rho_0 g(\rho_1/\rho_0\,\Delta h)}{2\beta \sin\gamma_0}\bigg|_{h_i} \tag{19}$$

evaluated at the altitude h_i of interest.

In solving Eq. (12) for γ_1, required to determine the impact range error R_1 according to Eq. (13), the assumption that (V_1/V_0) is the primary forcing term will again be made, and this results in the approximate relation

$$\gamma_1' \approx \frac{2g\cot\gamma_0}{V_0^2}\left(\frac{V_1}{V_0}\right) \tag{20}$$

It will be further assumed that the constant path angle, zero-gravity solution of Allan and Eggers[5] for the unperturbed velocity V_0 can be used in Eq. (20) to provide an adequate history of γ_1. Thus, using

$$V_0 = V_e \exp\left(\frac{-g\rho}{2\beta\alpha\sin\gamma_0}\right) \tag{21}$$

and again employing the constant path angle assumption for γ_0, Eq. (20) is integrated to yield the perturbed path angle γ_1 history as

$$\gamma_1(h) = -\frac{2g\cos\gamma_0(V_1/V_0)}{\alpha V_e^2 \sin\gamma_0}\left[\alpha(h_i - h) + \sum_{n=1}^{\infty}\frac{A^n}{n\cdot n!}(Z^n - Z_i^n)\right] \tag{22}$$

where A and Z are defined as

$$A = \frac{g\rho_s}{\alpha\beta\sin\gamma_0}; \quad Z = e^{-\alpha h} = \rho/\rho_s \tag{23}$$

where the i subscript defines the altitude h_i at which the influence coefficient a_{ρ_i} is to be determined. If Eq. (22) is used in Eq. (13) with the assumption of constant path angle γ_0, the range deviation R_1 is obtained as

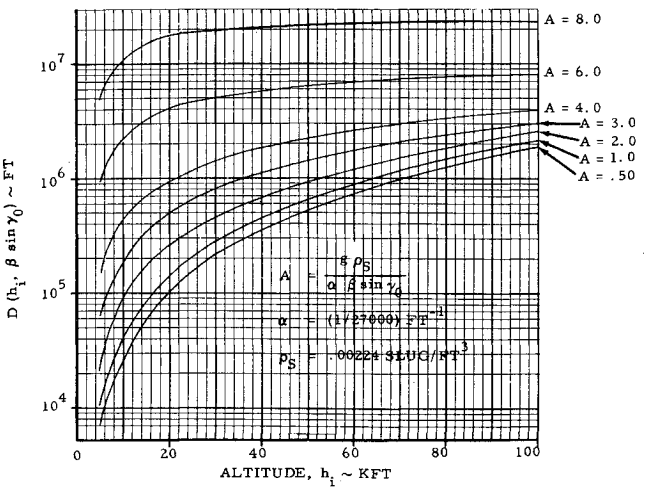

Fig. 3 Density influence coefficient parameter, $D(h_i, \beta \sin\gamma_0)$.

$$R_1 = -\frac{2g\cot\gamma_0(V_1/V_0)}{\alpha V_e^2 \sin^2\gamma_0}\left\{\frac{-\alpha h_i^2}{2} + \sum_{n=1}^{\infty}\frac{A^n}{n\cdot n!}\times \left[\frac{-1}{n\alpha}(1-e^{-n\alpha h_i}) + h_i e^{-n\alpha h_i}\right]\right\} \quad (24)$$

Employing the relation for (V_1/V_0) given by Eq. (19) and the definition of the density influence coefficient given by Eq. (14), there results for the influence coefficient a_{p_i} at altitude h_i

$$a_{p_i} = -\frac{\rho_0 g^2 \cos\gamma_0}{\alpha\beta V_e^2 \sin^4\gamma_0} D(h_i, \beta\sin\gamma_0) \quad (25)$$

where

$$D(h_i, \beta\sin\gamma_0) \doteq \frac{\alpha h_i^2}{2} + \sum_{n=1}^{\infty}\frac{A^n}{n\cdot n!}\left[\frac{1}{n\alpha}(1-e^{-n\alpha h_i}) - h_i e^{-n\alpha h_i}\right] \quad (26)$$

The term denoted as $D(h_i, \beta\sin\gamma_0)$ is a function of altitude and trajectory parameter $\beta\sin\gamma_0$ only. This term has been evaluated numerically (Fig. 3) for altitudes below Kft and for a range of trajectory conditions $\beta\sin\gamma_0$.

The parameter A is defined to coincide with Glover's trajectory parameter K_{SL}. The atmospheric model used in generating the results shown in Fig. 3 was $\rho_S = 0.00224$ slug/ft^3 and $\alpha = (1/27000)\,\text{ft}^{-1}$. This selection is somewhat arbitrary and was made in an attempt to minimize in some sense the integrated error of $(1/V_0^2)$ in Eq. (20). The results given by Eq. (25) and Fig. 3 indicate that for very large values of β (small A), the density influence coefficients will vary nearly inversely with β for given re-entry conditions. For lower values of β (A larger than about 2–3) the differences in the parameter $D(h_i, \beta\sin\gamma_0)$ will become more significant. A comparison of numerical point mass and approximate results is given following the derivation of the wind influence coefficients.

Wind-Induced Impact Dispersions

The primary effect of a horizontal in-plane (head) or out-of-plane (cross) wind will be to cause a misalignment of the drag force orientation. The missile will then drift with the wind. This effect is first considered for a crosswind. Referring to Fig. 1 and Eq. (8), the cross range velocity relation is, for small wind induced misalignments η,

$$V_x' = \frac{-q_0 g}{\beta V_0 \sin\gamma_0}\left(\frac{w_\perp - V_x}{V}\right) \quad (27)$$

Equation (27) is integrated to yield the cross range velocity V_{x_e} at the end of the interval

$$V_{x_e} = w_\perp\left[1 - \exp\left(\frac{-g(\rho_L - \rho_H)}{2\alpha\beta\sin\gamma_0}\right)\right] \quad (28)$$

If the interval is small, the previous equation can be approximated by

$$V_{x_e} \approx \left.\frac{\rho_0 g(w_\perp \Delta h)}{2\beta\sin\gamma_0}\right|_{h_i} \quad (29)$$

Following the perturbation interval, $w_\perp = 0$ and Eq. (29) reduces to

$$V_x' = \rho g V_x / 2\beta\sin\gamma_0 \quad (30)$$

By using Eq. (5) with gravity effects neglected, Eq. (30) is rewritten as

$$V_x'/V_x = V_0'/V_0$$

which shows that the cross-range velocity ratio V_x/V_0 remains nearly constant during re-entry. With this result and the assumption of constant path angle γ_0, Eq. (9) is integrated to yield

$$X = -\left(\frac{V_{x_e}}{V_0}\right)\frac{h_i}{\sin\gamma_0} \quad (31)$$

Combining this with Eq. (29) and the definition of the cross-range wind influence coefficient,

$$a_{c_i} = X/w_\perp \Delta h \quad (32)$$

yields

$$a_{c_i} = \left.\frac{\rho_0 g h}{2\beta V_0 \sin^2\gamma_0}\right|_{h_i} \quad (33)$$

where the nominal trajectory parameters ρ_0, V_0, and γ_0 are evaluated at the altitude of interest h_i. In calculating values of a_{c_i} using Eq. (33), the densities ρ_0 should be taken from the actual profile being considered, and not from the exponential approximation. This also applies to usage of Eq. (25), since the perturbations in both cases are considered essentially as impulses which depend on the local values of density. Although an exponential approximation may provide adequate results for quantities for which density errors may be integrated out (e.g., velocity), local errors in density may be of the order of 20% in some instances.

In assessing the influence of a parallel wind on impact range error, it is assumed that the path angle deviation occurring during the wind perturbation interval remains nearly constant thereafter. Accordingly, the second term of Eq. (6) may be used to obtain the path angle deviation γ_{1_e} present at the end of the perturbation. Taking constant properties during the interval, and assuming that w_p is large relative to V_p, there results

$$\gamma_{1_e} = \frac{-g\rho_0[1 + (2w_p/V_0)\cos\gamma_0](w_p \Delta h)}{2\beta\sin\gamma_0} \quad (34)$$

Using Eq. (34) in Eq. (13) with γ_0 taken as constant from h_i to impact, the parallel wind influence coefficient is obtained as

$$a_{p_i} = \left.\frac{g\rho_0 h[1 + (2w_p/V_0)\cos\gamma_0]}{2\beta V_0 \sin^2\gamma_0}\right|_{h_i} \quad (35)$$

This form differs slightly from Eq. (33). In the present case the effect of wind on dynamic pressure may be of first order, whereas for a crosswind it is of second order. For most cases of interest, the nonlinear term in Eq. (35) may be ignored, as may deviations in γ_1 following the perturbation. The cross and parallel wind influence coefficients are then approximately equal, and Eq. (33) may be applied for either type of wind effect.

Results—Wind and Density

Comparisons of wind and density influence coefficients as calculated from Eqs. (33) and (25) and as obtained from numerical integration of Eqs. (5–9) are presented in Figs. 4 and 5. All trajectories were begun at 100,000 ft with a velocity of 23,000 fps and path angle of 25°. Ballistic coefficients of 500, 1000, 2000, and 5000 psf were used and taken as constant throughout the trajectory. The atmospheric model used in the numerical integrations was a 1966 15° N latitude standard atmosphere.[6] The point mass program employed was set up to calculate the approximate influence coefficients as part of the unperturbed trajectory simulation. Instantaneous values of V_0 and γ_0 were used in the calculations. The values of density were taken from the standard atmospheric model and not from the exponential approximation.

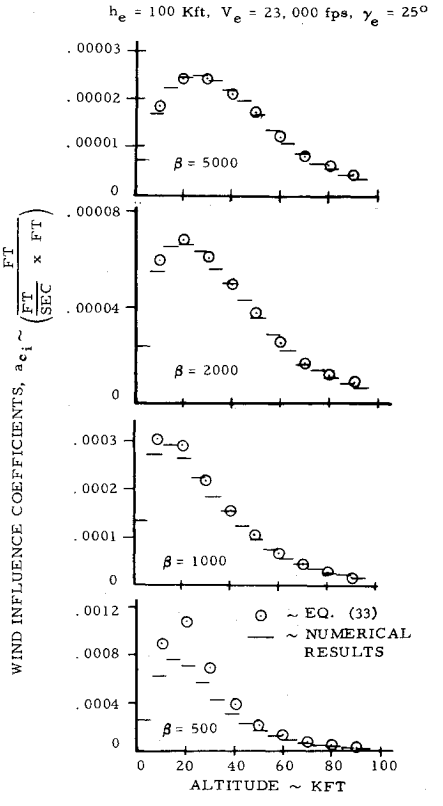

Fig. 4 Comparison of numerical and approximate wind influence coefficient results.

The comparison in Fig. 4 shows excellent agreement between approximate and numerically determined wind influence coefficients for ballistic coefficients of 1000, 2000, and 5000. Fair agreement is exhibited for the $\beta = 500$ case. Note that the altitude of peak influence coefficient varies from ~25 kft ($\beta = 5000$) to near 15 kft ($\beta = 500$). The case shown represent a range in the trajectory parameter A (Glover's K_{SL}) of 0.92–9.2.

The agreement between approximate and numerically obtained density influence coefficients (Fig. 5) is excellent for the $\beta = 2000$ and 5000 cases, good for $\beta = 1000$, and very poor for $\beta = 500$. The discrepancy in the latter case is a result of neglecting gravity and changes in path angle in the analysis leading to Eq. (25).

The previously mentioned results indicate that for vehicles with ballistic coefficients constant (or nearly so) throughout re-entry, the wind influence coefficients can be calculated adequately using Eq. (33) for values of trajectory parameter A up to at least 9. The associated density influence coefficients can be obtained for values of A less than approximately 5. It appears likely that in studying vehicles with drag dependence on Mach number, the basic Eqs. (25) and (33) could be used to scale known influence coefficient profiles (assumed numerically determined) to cases for different entry conditions (V_e, γ_e) and ballistic coefficients β.

Formulation of Angle of Attack Statistical Effects

In addition to dispersions resulting from atmospheric effects, impact errors will also derive because all vehicles of a given re-entry system will not enter at identical angles of attack. The respective drag histories throughout descent will therefore vary due to the differing angle of attack histories. The resulting dispersion magnitudes will be of importance in determining allowable tolerances on the system used to orient the vehicle prior to re-entry. A simple approach to this problem is presented in order that impact dispersions can be estimated for a specified re-entry system without recourse to the usual Monte-Carlo-type analysis.

The angle of attack at very high altitudes, where atmospheric effects are negligible, will generally be composed of a component due to the drift in re-entry vehicle attitude following separation (the body fixed high-frequency component, in the sense of Nelson[7]) and a precessional component about the drift, resulting from the spin stabilization maneuver. Both components are damped during descent through the atmosphere, as described, for instance, by Platus[8] and Leon.[9]

It will be assumed in this analysis that either one component or the other is dominant, i.e., that the total angle of attack δ is composed of a mean which is slowly varying as the missile descends, and about which any oscillations are of small amplitude. In this case it is plausible to postulate that the orthogonal angle of attack components θ and ψ will be statistically independent, normally distributed, and with zero mean values. The distribution for the initial total angle of attack $\delta_e = (\theta_e^2 + \psi_e^2)^{1/2}$ is then given by a Rayleigh distribution[10]

$$f(\delta_e) = \frac{\pi \delta_e}{2\delta_m^2} \exp\left(\frac{-\pi \delta_e^2}{4\delta_m^2}\right) \tag{36}$$

where δ_m, assumed known, is the mean value at initial re-entry. This distribution is completely characterized by specification of the mean δ_m. It is now desired to utilize Eq. (36) in order to obtain the vehicle drag characteristics in terms of the parameter δ_m. This is done by noting that in many cases the total drag of a vehicle at angle of attack δ may be represented adequately as

$$C_D(\delta) \approx C_D(\delta = 0) + K\delta^2 \tag{37}$$

Defining the increment in drag due to angle of attack as $C_{D_1} = K\delta^2$, and utilizing the relation[10]

$$f(C_{D_1}) = f(\delta_e) \Big/ \left|\frac{dC_{D_1}}{d\delta_e}\right| \tag{38}$$

which applies generally provided that δ_e is a single valued function of C_{D_1}, the probability density of the drag increment C_{D_1} at initial re-entry is obtained as an exponential distribution

$$f(C_{D_1}) = \frac{\pi}{4K\delta_m^2} \exp\left(\frac{-\pi C_{D_1}}{4K\delta_m^2}\right) \tag{39}$$

The mean value is given simply as[10]

$$\langle C_{D_1} \rangle = 4K\delta_m^2/\pi \tag{40}$$

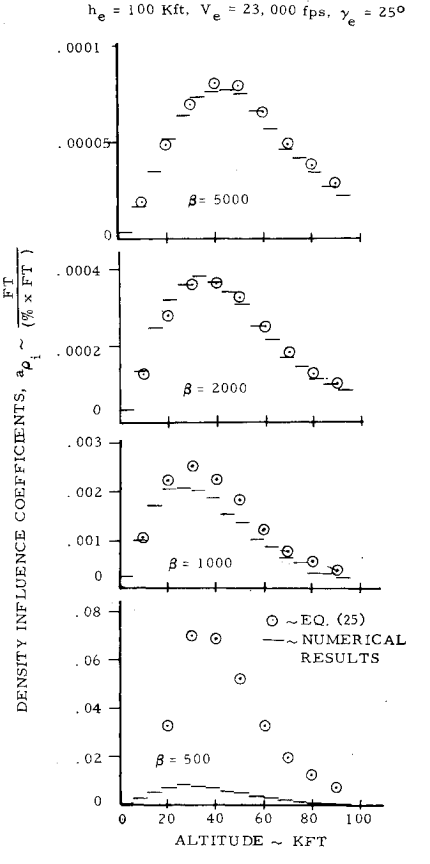

Fig. 5 Comparison of numerical and approximate density influence coefficient results.

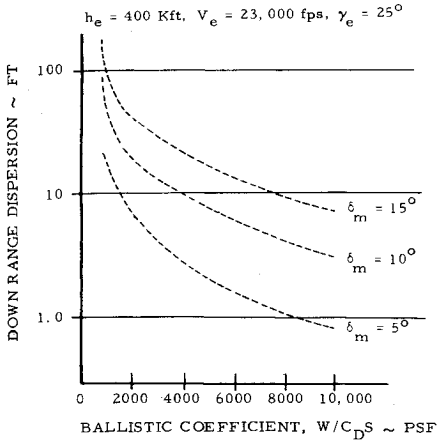

Fig. 6 Effect of ballistic coefficient on angle of attack induced dispersion.

Thus the drag increment C_{D_1} at re-entry may be described completely by the mean initial re-entry angle of attack δ_m.

In calculating the $1-\sigma$ error in C_{D_1}, the second moment about the mean would normally be taken. However, it is desirable that the "error" conform to that obtained from other sources, such as atmospheric effects, which are assumed normally distributed. Therefore, the "error" will be defined here as that value which encompasses 68.34% of the area about the mean of the probability density function $f(C_{D_1})$, thus defining an equivalent normal distribution $1-\sigma$ error. This is defined by the relation

$$\int_{\langle C_{D_1}\rangle - \sigma C_{D_1}}^{\langle C_{D_1}\rangle + \sigma C_{D_1}} f(C_{D_1})\,dC_{D_1} = 0.6834 \tag{41}$$

This relation is integrated and solved for σC_{D_1} to yield

$$\sigma C_{D_1} = 1.05K\delta_m{}^2 \tag{42}$$

Equation (42) represents an equivalent $1-\sigma$ error in drag increment C_{D_1} at initial re-entry (e.g. at 300 kft). The result must be defined at other altitudes, as the vehicle descends and the angle of attack is attenuated.[8,9] This is done by employing the initial assumption that throughout entry the mean total angle of attack is large relative to oscillations about the mean. This implies that the total angles of attack for any two vehicles under consideration will maintain a constant ratio throughout re-entry. Thus, if an attenuation factor $\lambda(h)$ is defined, i.e., $\delta(h) = \lambda(h)\delta_e$, the same for all vehicles, the history of equivalent $1-\sigma$ error in incremental drag C_{D_1} is obtained as

$$\sigma C_{D_1}(h) = 1.05K\lambda^2(h)\,\delta_m{}^2 \tag{43}$$

To obtain the resulting $1-\sigma$ impact range error it is noted that, within the assumptions made, the variables C_{D_1} at various altitudes will be perfectly correlated, i.e., for two altitude levels i and j [in the sense of Eq. (1)]

$$COV(C_{D_{1_i}}, C_{D_{1_j}}) = \sigma C_{D_{1_i}}\sigma C_{D_{1_j}} \tag{44}$$

This will be true provided that the damping characteristics of the system are not considered as statistical variables, i.e., all vehicles are assumed to possess identical damping. Violation of this assumption should not result in a significant compromise of the analysis, since the primary damping mechanism at high altitudes is the increasing density,[9] whose effect will, in fact, be substantially identical for all vehicles.

Equation (44) above permits the range error to be obtained simply by performing two point mass computer simulations using alternately the mean and the mean $+1-\sigma$ incremental drag in addition to the basic vehicle drag. The angle of attack attenuation $\lambda(h)$ to be used can be obtained from a single six-degree-of-freedom simulation for a vehicle with representative properties, or by use of the simple relations as given, for example, in Refs. 8–9. This procedure is certainly much simpler than the usual Monte-Carlo statistical approach. An alternate procedure would be to compute a history of the relative drag error $[\sigma C_{D_1}/C_D$ $(\delta = 0)]$ and use the density influence coefficients given by Eq. (25), according to the relation

$$\sigma_\delta = \sum_{i=1}^{n}\left(\frac{\sigma C_{D_1}}{C_{D_0}}\right)a_{\rho_i}\Delta h_i \tag{45}$$

However, it might prove necessary to utilize an alternate atmospheric density model than used previously, since the primary angle-of-attack contributions to dispersion will occur at very high altitudes. The model used earlier was specifically for altitudes below 100 kft, where nearly all of the wind and density induced dispersions are produced.

Some results obtained with the former technique (point mass simulations) are shown in Fig. 6 for various assumed mean re-entry angles of attack and ballistic coefficients. The dispersion is quite sensitive to ballistic coefficient and varies with mean angle of attack approximately as $\delta_m{}^2$. Information such as shown in Fig. 6 should prove useful in the performance of studies designed to establish the tradeoffs between mean-initial entry angle of attack, ballistic coefficient, and dispersion magnitude.

Conclusions

The derivation of wind and density impact dispersion influence coefficients has been presented. The primary objective has been to simplify the procedures used in obtaining atmospheric dispersions, particularly by obviating the need for a large number of point mass trajectory simulations which are normally performed to determine numerically the influence coefficients. The results have been shown to be valid for a wide enough range in vehicle characteristics that they should prove useful, especially for design studies where a large number of cases must be considered.

The influence of the statistical nature of re-entry angle of attack upon dispersion has also been derived in an approximate manner. As with the atmospheric effects, the establishment of simple, usable relations was emphasized, rather than the maintenance of mathematical rigor. The angle of attack induced impact error can be calculated by employing two point mass trajectory simulations, with the basic damping characteristics the only additional information required.

Other symmetric vehicle effects which have not been dealt with specifically, such as changes in weight or statistical variation of the drag coefficient during entry, can be assessed by using the relations derived for the density influence coefficients. Thus, the relations presented herein provide a useful means of establishing the impact dispersions resulting for most symmetric re-entry vehicle effects of interest.

References

[1] Crenshaw, J. P., "Effect of Lift with Roll Rate Variation on Re-Entry Vehicle Impact," *Journal of Spacecraft and Rockets*, Vol. 8, No. 5, May 1971, pp. 483–488.

[2] Valley, S., ed., *Handbook of Geophysics and Space Environments*, McGraw-Hill, New York, 1965, Chap. 3.

[3] Finarelli, H., "Statistical Roll Resonance Computer Program—Second Generation," GE TIS 68SD324, Nov. 1968, General Electric Co., Philadelphia, Pa.

[4] Glover, L. S., "Approximate Equations for Evaluating the Impact Dispersion Resulting from Re-Entry Winds and Deviations in Density," TG 1132, Sept. 1970, The Johns Hopkins Univ., Silver Spring, Md.

[5] Allen, H. J. and Eggers, A. J., "A Study of the Motion and Aerodynamic Heating of Ballistic Missiles Entering the Earth Atmosphere at High Supersonic Speeds," Rept. 1381, 1958, NACA.

[6] *U.S. Standard Supplements*, Table 5.2, U.S. Govt. Printing Office, Washington, D.C., 1966.

[7] Nelson, R. L., "The Motions of Rolling Symmetrical Missiles Referred to a Body Axis System," TN 3737, Nov. 1956, NACA.

[8] Platus, D. H., "Angle-of-Attack Convergence and Windward-Meridian Rotation Rate of Rolling Re-Entry Vehicles," *AIAA Journal*, Vol. 7, No. 12, Dec. 1969, pp. 2324–2330.

[9] Leon, H. I., "Angle-of-Attack Convergence of a Spinning Missile Descending Through the Atmosphere," *Journal of Aerospace Sciences*, Vol. 23, No. 8, Aug. 1958, pp. 480–484.

[10] Parzen, E., *Modern Probability Theory and Its Applications*, Wiley, New York, 1960, p. 312.